Energy and Buildings 123 (2016) 50–58

Contents lists available at ScienceDirect

Energy and Buildings

journal homepage: www.elsevier.com/locate/enbuild

Thermal and hydraulic analysis on a novel Trombe wall with venetian blind structure

Wei He [a,*], Xiaoqiang Hong [b], Xiaoling Wu [b], Gang Pei [b], Zhongting Hu [b], Wenxue Tang [c], Zhihe Shen [a], Jie Ji [b]

[a] Department of Building Environment and Equipment, Hefei University of Technology, Hefei 230009, China
[b] Department of Thermal Science and Energy Engineering, University of Science and Technology of China, Hefei 230026, China
[c] Guangdong Fivestar Solar Energy Co., Ltd., DongGuan 523051, China

ARTICLE INFO

Article history:
Received 18 January 2016
Received in revised form 10 April 2016
Accepted 17 April 2016
Available online 22 April 2016

Keywords:
Trombe wall
Nusselt number
Friction factor
CFD
Heat transfer
Venetian blinds

ABSTRACT

This paper aims to present a CFD investigation into the heat transfer and friction characteristic of a Trombe wall equipped with venetian blinds. This involved (1) development of a CFD model; (2) dedicated experiment for verification of the model; (3) modelling result analyses and conclusion. Based on experimental data, the model was validated and it was able to yield satisfactory predictions. The characteristics of the Trombe wall with venetian blinds inclined from 5° to 85° were investigated. The Nusselt number and friction factor for Reynolds number within the range of 4173–16,693 were also achieved in the simulation. Analyses of the research results indicated that smaller slat angle helps enhance the outlet air temperature and solar thermal efficiency, while increasing the Reynolds number leads to decrease in outlet air temperature and increase in solar thermal efficiency. The empirical equations of heat transfer and flow resistance were proposed. The Nusselt number value of the venetian blind increases with the increase of the Reynolds number value and decrease of the slat angle. In addition, the Nusselt number is proportional to the range of 0.422–0.461 power of the Reynolds number. The friction factor value decreases with the increase of the Reynolds number value and the slat angle.

1. Introduction

Building sector is a big consumer of energy in China, approximately 25–30% of total energy consumption. This is mainly due to the large amount of energy used for cooling and heating so as to achieve an optimal thermal performance and an acceptable condition of comfort in the buildings [1]. Although the proportion is lower than developed countries, it is believed that it will increase to a higher level due to people's demand for better life with the rapid development in China [2,3]. China has been classified into five climate zones that comprise the very cold zone, cold zone, hot summer and cold winter zone, hot summer and warm winter zone and mid zone. Hefei in Anhui province that located in central china (117.25°E and 31.83°N), belongs to the hot summer and cold winter climatic region with the average temperature in the coldest month varying from 0° to 10 °C [4]. The heating temperature set point in the hot summer and hot winter climatic region is recommended to be a lower temperature range of 17–18 °C in winter than that predicted by the heat balance model (PMV/PPD) and ASHRAE's adaptive comfort model [5]. Applying solar energy is considered as one of the most efficient methods to reduce fossil energy consumption in the buildings, such as a Trombe wall.

Trombe walls, which are also known as an passive solar technology, reduces a building's energy consumption obviously [6]. An investigation [7] reported that energy heating needs can be reduced in 16.36% if a Trombe wall is added to the building envelope. And Shen et al. [8] found that the Trombe wall has better energetic performances than the classical wall in cold and cloudy weather through the comparisons between the simulation results of a classical Trombe wall and a composite Trombe wall. Moreover, Trombe wall has some unique features, such as low cost, simple geometry and reliable operation. Many studies on different types of Trombe wall have been carried out and reported.

Rabani et al. developed an unsteady 2D numerical model of the Trombe wall and indoor air environment to investigate the time duration of room heating during the non-sunny periods [9]. Using phase-change material in a Trombe wall is also proposed in order to enhance efficiency and decrease a building's dead load [10]. Zalewski et al. presented an experimental study of a small-scale Trombe wall containing the phase material and found that

* Corresponding author.
E-mail address: hwei@hfut.edu.cn (W. He).

http://dx.doi.org/10.1016/j.enbuild.2016.04.042
0378-7788/

Nomenclature

A	Effective absorbing area (m^2)
C_p	Specific heat capacity (J/kg-K)
G	Solar radiation intensity (W/m^2)
h	Heat transfer coefficient (W/m^2-K)
m	Mass flow rate (kg/s)
Q	Heat energy rate (W)
T	Temperature (K)
RE	Relative error
V	Wind speed (m/s)
X	Value

Greek letter

α	Absorption ratio
η	Efficiency
τ_c	Cover transmittance

Subscripts

exp	Experimental
th	Thermal
in	Inlet
out	Outlet
sim	Simulated

the 2.5 cm thick latent solar wall perform as well as a 15 cm concrete solar wall [11]. Khalifa and Abbas conducted a computerised dynamic simulation on a zone heated by a thermal storage wall. They examined three different storage material and concluded that an 8 cm thick storage wall made from hydrated salt is capable of maintaining the comfort temperature with the least room temperature fluctuation [12]. Another invention called PV-Trombe wall, which can produce electricity and heat simultaneously, has been theoretically and experimentally investigated by Ji et al. [13,14]. The air flows through the air duct and absorbs the PV heat, and thus increasing the PV efficiency and reducing the air-conditioning loads of the building [15–18]. In addition, the aesthetic value that the dark blue solar cells bring can increase the building's appeal, and thus help the spread and application of Trombe wall.

To further improve the performance of the Trombe wall systems, a novel Trombe wall with venetian blind structure is thereby proposed. Nowadays, venetian blinds are widely used in buildings to adjust the amount of incoming daylight. Use of venetian blind for Trombe wall is the only recent development. This combined system, as shown in Fig. 1, is able to improve the energy efficiency of heat collecting in winter and prevent over heating in summer by switching the working modes of the system. The solar rays are absorbed by the venetian blinds and inner wall. The air in the gap between the glazing and the inner wall is heated by the venetian blinds and inner wall, and then ejected into the room in winter mode or ejected to the outdoor in summer mode. The absorbed solar irradiance can be controlled by controlling the slat angle of the venetian blind installed between the glazing and the wall. In winter mode, it is necessary to provide enough fresh air to guarantee the indoor air quality as the air circulation through the Trombe wall would result in air quality degradation. Therefore the venetian blinds need to clean frequently. In previous studies, we analyzed the influence of the location of the venetian blind and the structural parameters on the thermal performance of the Trombe wall by using a 3-D CFD model [19]. We also developed a dynamic numerical model to study the thermal behavior of Trombe wall and its contribution to indoor thermal comfort and energy performance [20]. However, when modelling the convection heat transfer between the cavity air and venetian blinds, the venetian blinds were assumed to be long horizontal cylinder in the ambient fluid. In another words, we assumed that the slat angle does not affect the convection heat transfer coefficient on the venetian blinds and the friction factor along the air duct in the previous model.

To further understand the insights of the novel Trombe wall with venetian blind structure, a theoretical investigation into the effect of the different slat angles on the thermal efficiency, Nusselt number and friction factor of the Trombe wall will be carried out. The objective of this work is to establish heat transfer and fluid friction data for the Trombe wall. In this paper, the Reynolds number was arranged in the range of 4173–16,693.

2. Experimental setup

A prototype system was constructed in Hefei, China. The experimental platform was a simple room with Trombe wall on its south side, located at University of Science and Technology of China. The photograph of the prototype is shown in Fig. 2. The area of the Trombe wall is 2.00 m height × 1.00 m width. Between the glass and the internal wall, an air duct of 0.14 m width was left. And the venetian blind was installed in the middle of the air duct, which can be inclined at range of −90 ° to 90° from the horizon to control the rate of solar radiation striking on the slats. There were two air vents at the upper and the lower positions of the internal wall. The vents are both 0.40 m width and 0.10 m high, one was located at 0.10 m below the top of the Trombe wall, and another was located at 0.10 m away from the bottom of the wall.

In the experiment: A anemometer(kanomax A533-type) whose measurement accuracy is 0.01m/s was used to record air mass flow rate, A pyranometer was installed to measure the vertical solar radiation, i,e., the same south-facing vertical surface position as the Trombe wall. At the same time, we used three thermocouples to measure the outdoor, Trombe wall bottom vent and top vent air temperature. The measured vertical solar radiation, inlet and outlet temperatures measured on January 5, 2014 are shown in Fig. 3. During the test procedure, the slats were inclined at 45° from the horizon. Another pyranometer was installed at the angle of 45° from the horizon to measure the total radiation intensity of the angle. And the air vents on the wall were opened while the air vent on the outer pane was closed.

3. Methodology

A CFD approach was employed to model the forced air flow and heat transfer in the Trombe wall. Fig. 4 designates the computational domain for the Trombe wall with venetian blind structure in winter operation. It was a two-dimensional model. A computational grid of approximately 0.35 million quadrilateral cells was created. Besides the near-wall mesh was refined to improve robustness and accuracy. In the computation, continuity, momentum and energy equations of air are solved in the domain using Fluent for the steady flow analysis [21].

The fluid is considered incompressible with constant thermophysical properties except for the air density, which is treated using the Boussinesq approximation, and the flow is assumed to be turbulent, steady, two-dimensional and with no viscous dissipation.

The inlet, ambient and the wall boundary condition were specified using the measured data (Fig. 4) for numerical solution. In the glass panel and venetian blinds, the conduction heat transfer equations are solved, wherein the blinds act as absorbers of solar radiations. The glass panel was set as convective wall boundary. Taking the effects of free convection and radiation into account, the convection coefficient at the glass panel is given by [22]

$$h = 5.7+3.8V \quad (1)$$

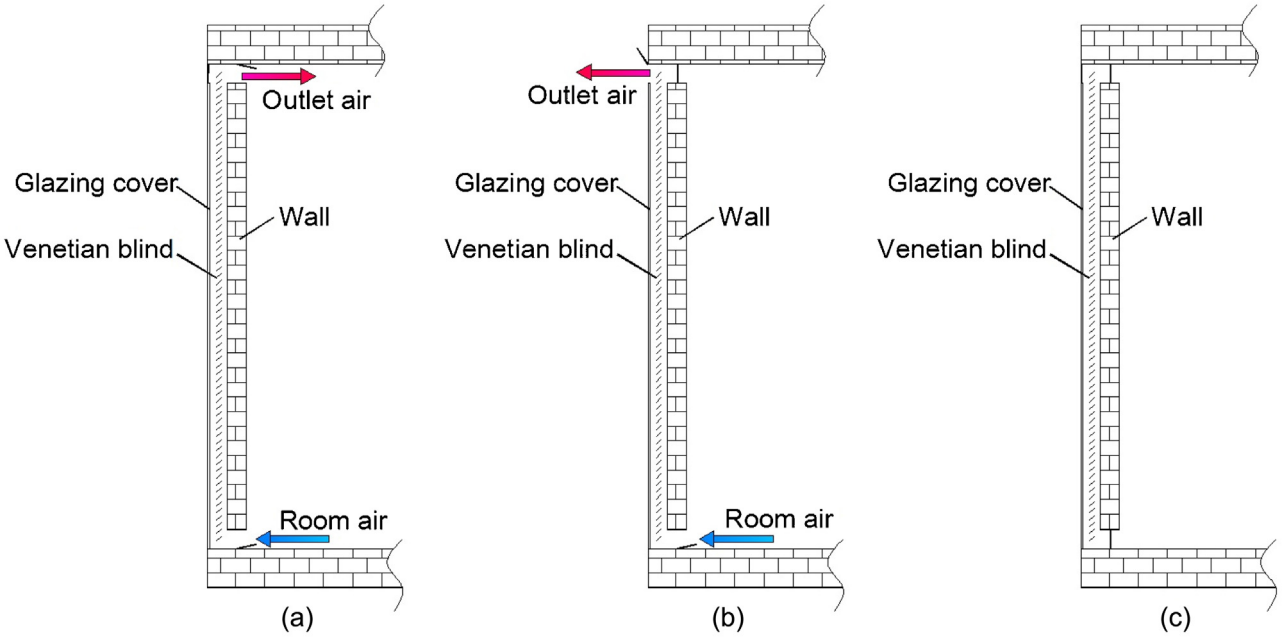

Fig. 1. Schematic of the Trombe wall with venetian blind structure: (a) winter mode; (b) summer mode; (c) without ventilation mode.

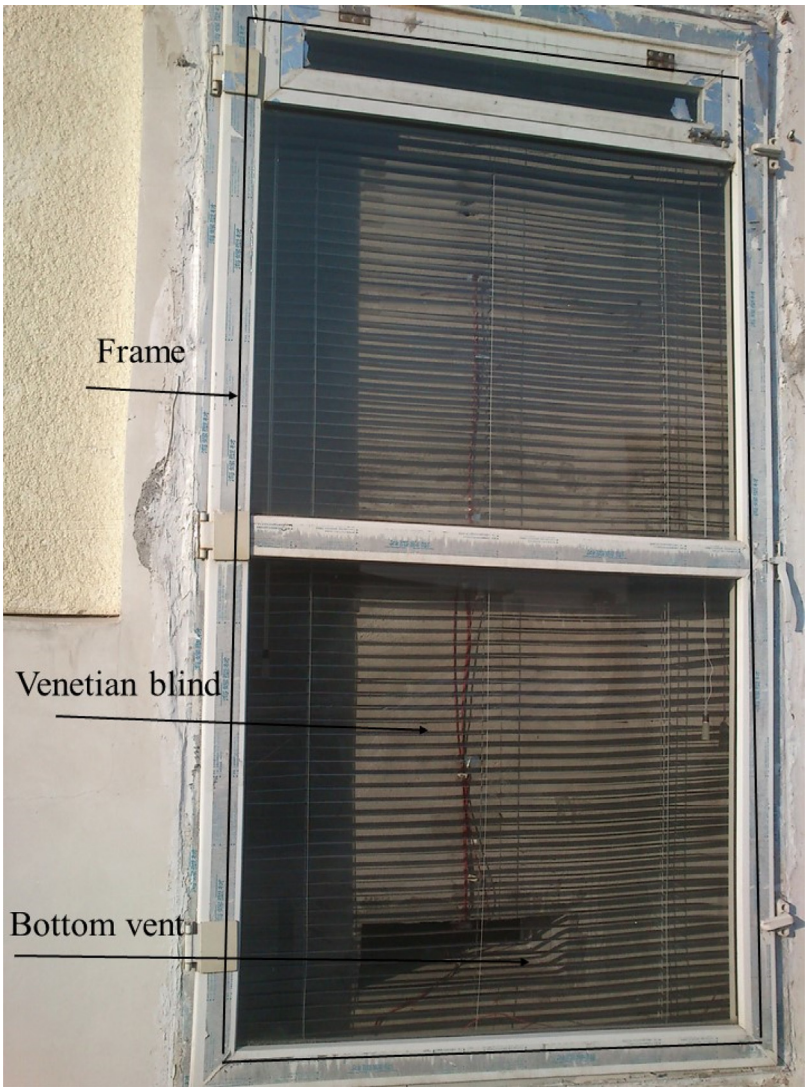

Fig. 2. Photograph of the prototype.

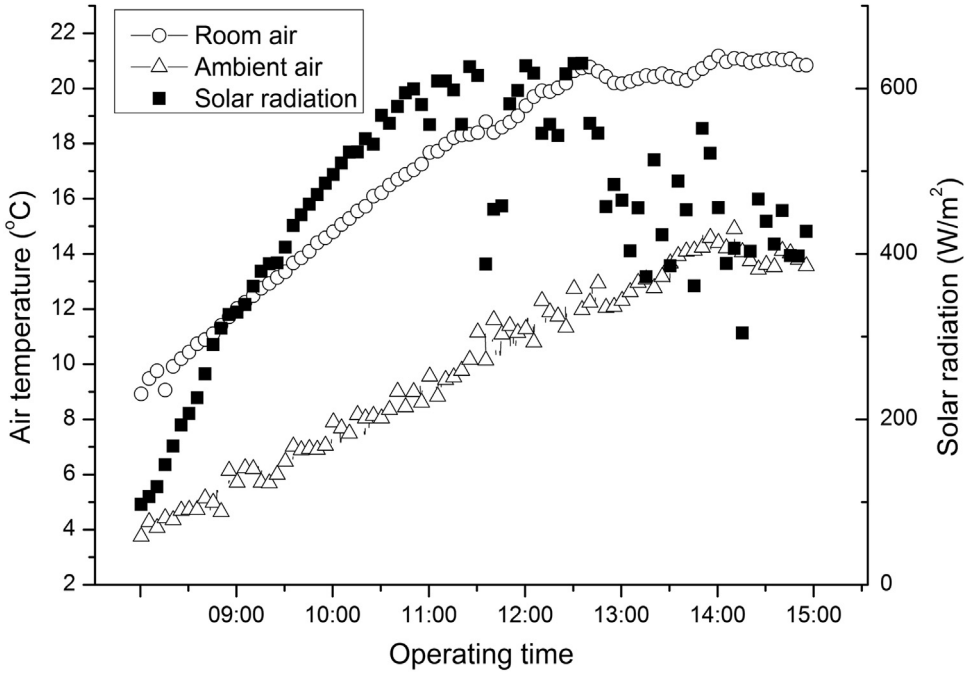

Fig. 3. Solar radiation and air temperature measured over the testing day duration.

where V is the wind speed in m/s. The ambient temperature is known using the measured data. A constant heat flux was set on the blind, which was refer to as the solar energy absorbed by the blind and transferred to the above computational domain, while for other walls adiabatic boundary condition was applied. The heat energy absorbed is calculated as follows:

$$Q_{abs} = (\tau_c \alpha) G_{45} \tag{2}$$

where $(\tau_{c\alpha})$ is the effective transmittance-absorptance product, which can be measured by the experiment; G_{45} is the total radiation flux of plane inclined at the angle of 45°.

The no slip velocity boundary conditions at the surface of all layers are assumed. The air is extracted from the inlet vent through the outlet vent at the top of the internal wall by a fan. Therefore, the air inlet vent was set as velocity inlet boundary and the outlet vent was set as pressure outlet boundary. The turbulence model of KOM was used to simulate the turbulence flow in the wall. The values of the turbulent kinetic energy and dissipation rate at the inlet and outlet depend on the turbulence intensity, length scale and inlet velocity.

The radiation heat transfer was calculated using surface-to-surface (S2S) radiation model. The SIMPLE algorithm was used for the velocity-pressure coupled relations among the governing equations. The upwind scheme was applied for the convective term. The simulation was first run without the S2S radiation model until convergence. After that, the simulation was continue run with the S2S model. The solution was considered converged when the residuals of the energy term and the other parameters were smaller than 10^{-6} and 10^{-4} respectively.

4. Model validation

To validate the model, the computer model was adjusted and operated at the identical conditions as to the outdoor weather data and the system's geometrical/operational parameters. The numerical solutions were then compared with the corresponding experimental results. To identify the discrepancy between the theoretical and experimental results, the root mean square percentage deviation (RE) was applied, given by:

$$RE = \sqrt{\frac{\sum \left[100 \times \left(X_{\exp} - X_{sim}\right) / X_{\exp}\right]^2}{\mathrm{n}}} \tag{3}$$

where n is the number of experiments implemented; X_{exp} and X_{sim} are the experimental and simulated values respectively.

In this paper, the solar thermal efficiency of Trombe wall is defined as the ratio of the heat absorbed by the air to the solar energy strikes on the south wall for the purpose of the model validation, as follows. It should be mentioned that a precise definition of the solar thermal efficiency of Trombe wall in mechanical ventilation mode should take the fan electrical consumption and heat transfer by conduction through the wall into consideration.

$$\eta = \frac{Q_{th}}{G_{90} \cdot A} \tag{4}$$

where A is the effective absorbing area of 1.7 m^2; G_{90} is the vertical solar radiation; Q_{th} is the heat absorbed by the air in the cavity, kJ, which can be calculated as follows:

$$Q_{th} = m \cdot C_p (T_{out} - T_{in}) \tag{5}$$

where m is the air mass flow through the solar collector, kg/s; C_p is the specific heat capacity of air, J/kg K; T_{out} is the temperature of the outlet air flow, °C; T_{in} is the temperature of the inlet air flow °C.

A comparison of the outlet air temperature and solar thermal efficiency obtained through CFD simulation and experimental measurements is displayed in Fig. 5. An excellent mutual agreement between modelling and testing is observed, with the mean temperatures of 25.50/25.38 °C for outlet air and average solar thermal efficiency of 57.31%/55.98%, while the corresponding deviations are 2.07% and 8.05% respectively. It could be found that the Trombe wall can provide warm air with the mean temperature of 25 °C, which is much higher that the acceptable temperature of residents in the hot summer and cold winter region in winter. The outlet air temperature and efficiency presented the similar variation trend, giving the up-rising trend in morning and down-falling trend in afternoon.

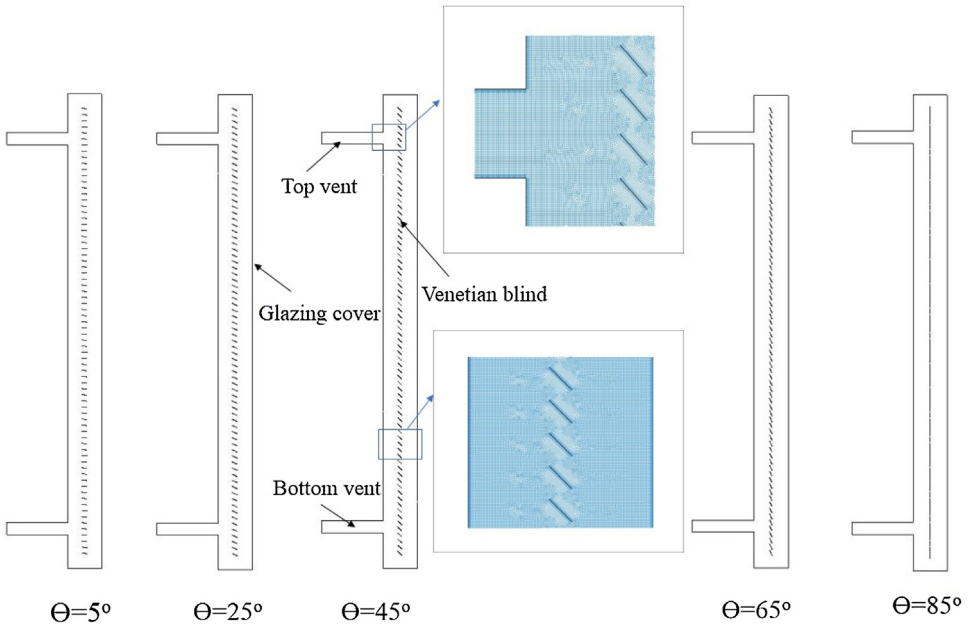

Fig. 4. Numerical Domain of the Trombe wall.

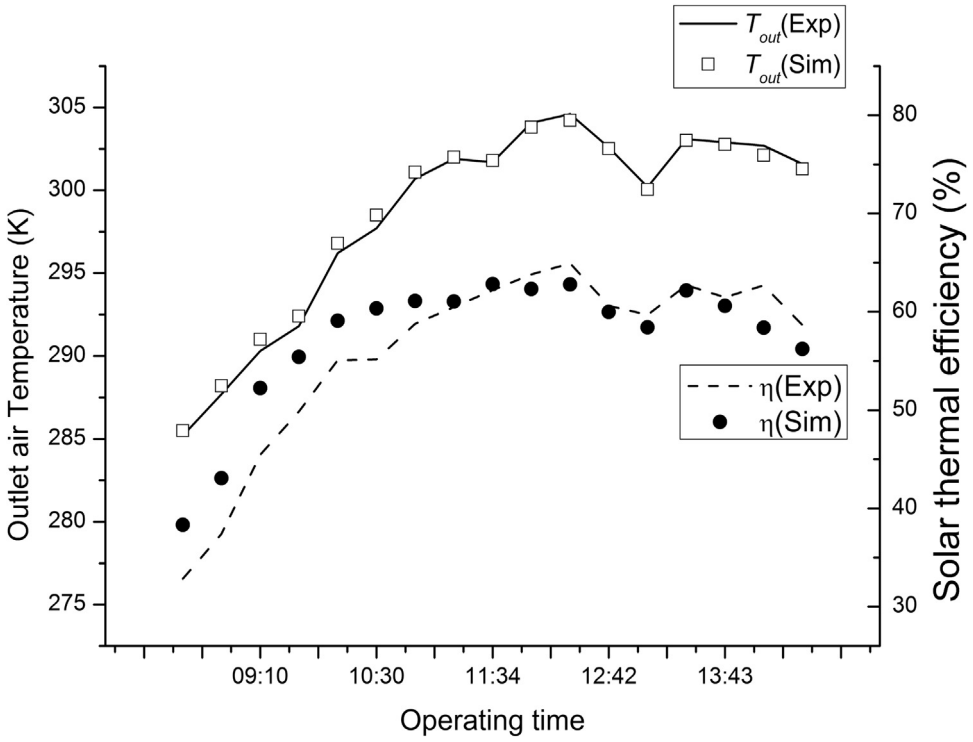

Fig. 5. The outlet air temperature and system's thermal efficiency.

The CFD model was therefore confirmed to give accurate prediction of system performance.

5. Results and discussion

The performance of the Trombe wall with venetian blind structure is affected by the geometry of its components. The present study mainly evaluates the influence of slat angle on the flow and heat transfer. For the different slat angles, while keeping the above system structure and boundary conditions constant, simulation was carried out using the established CFD model, and the results were obtained for outlet air temperature, solar thermal efficiency, Nusselt number and friction factor at eight level of Reynolds number in the range of 4173–16,693. The results obtained are illustrated as below:

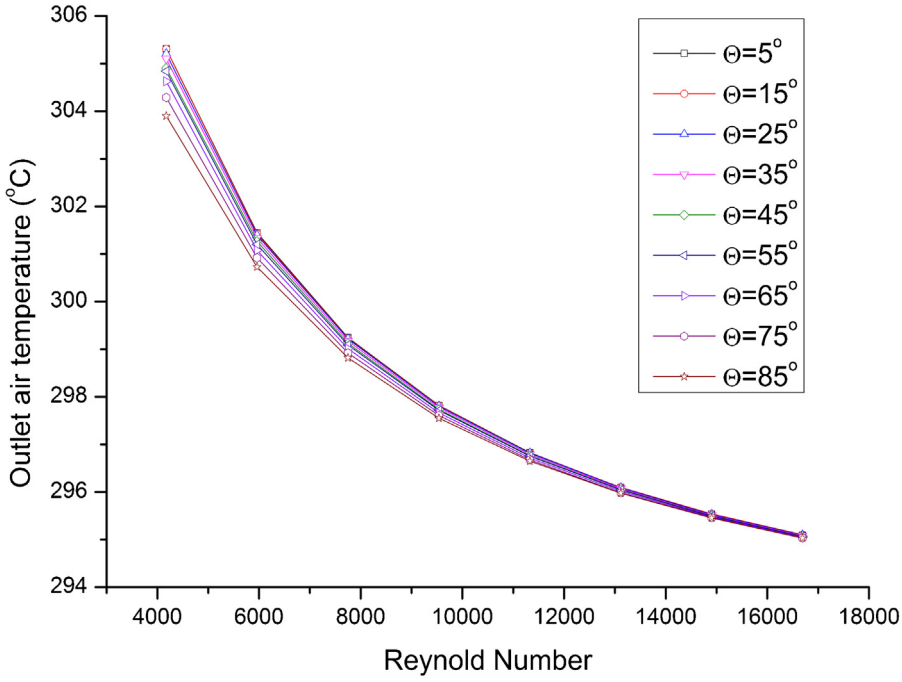

Fig. 6. Outlet air temperature versus Reynolds number for different slat angles.

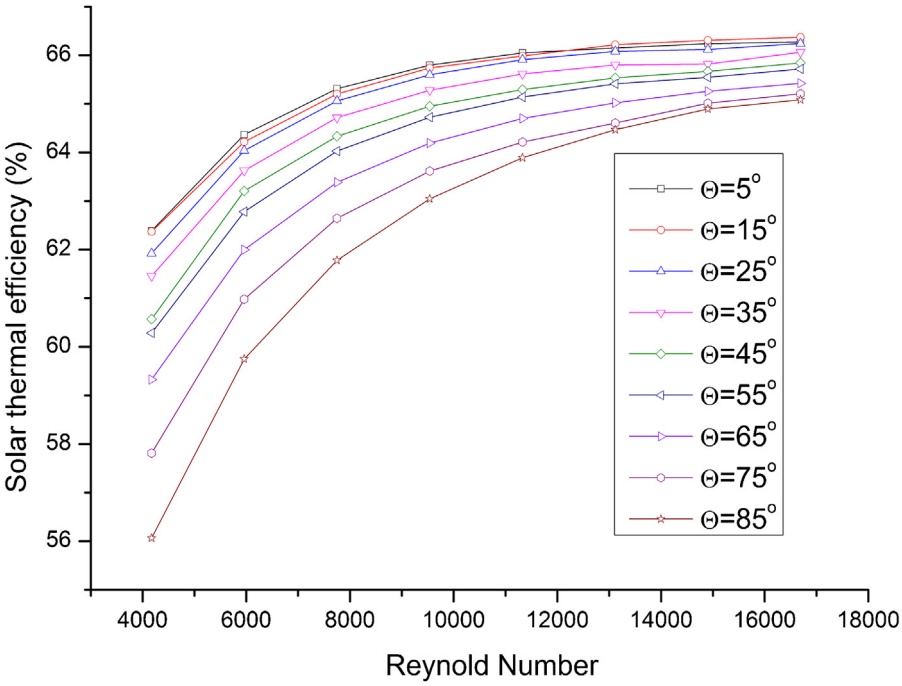

Fig. 7. Solar thermal efficiency versus Reynolds number for different slat angles.

5.1. Outlet air temperature and efficiency vs. slat angle and Reynolds number

Fig. 6 and 7 show the outlet air temperature and solar thermal efficiency versus Reynolds number for different slat angles. It can be seen that increasing the slat angle resulted in decrease in outlet air temperature and in associated thermal efficiency for Reynolds number in the range of 4173–11,327. For Reynolds number above 13,116, the outlet air temperature and thermal efficiency increase slightly firstly with the slat angle increasing from 5° to 10°, and afterwards they experience a decreasing trend with the increased of the slat angle. Therefore, with the same solar radiation received by venetian blinds, the slat angle is recommended to be smaller in order to enhance the heat transfer performance. It can be seen that increasing the Reynolds number (from 4173 to 13,116) would lead to decrease in the outlet air temperature and thermal efficiency for any slat angle. Therefore, using the fan at high flow rate will help improve the system's thermal efficiency. Meanwhile, the increasing of the air mass flow rate would decrease the air temperature of outlet vent and indoor thermal comfort, which is very important

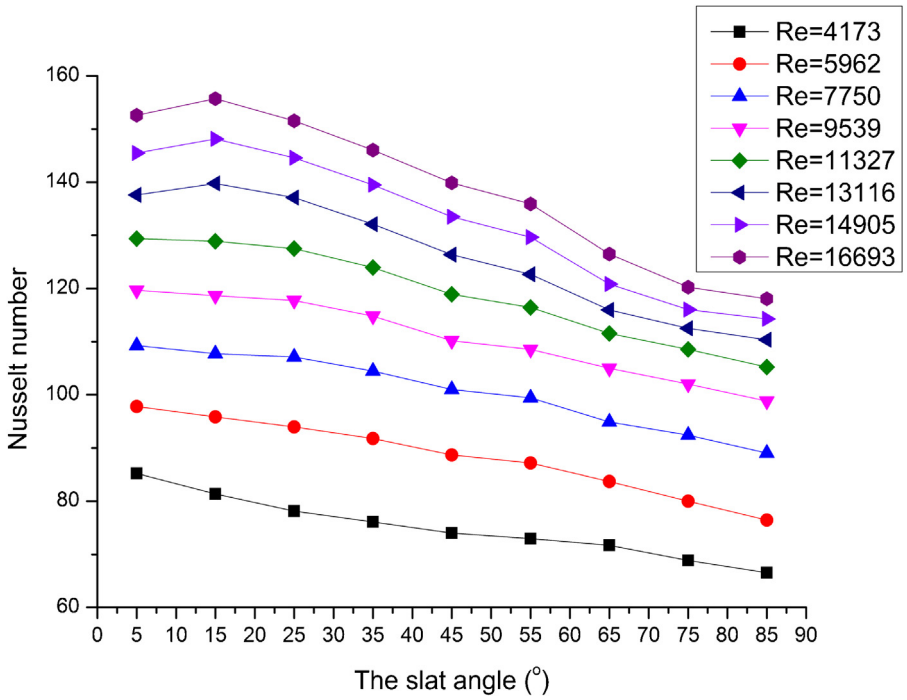

Fig. 8. Dependence of Nusselt number on the slat angle.

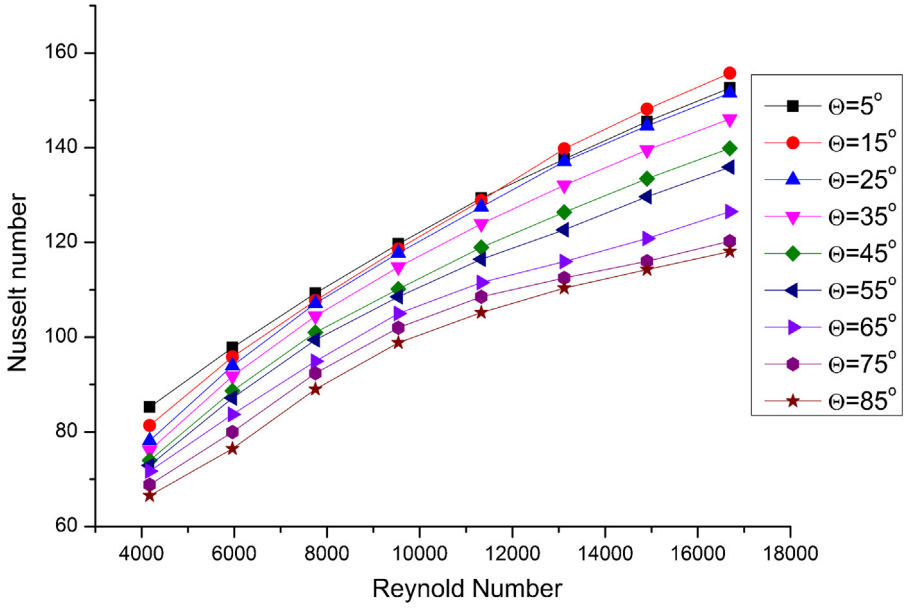

Fig. 9. Dependence of Nusselt number on Reynold number.

for the application of the Trombe wall. It is critical to set a suitable fan speed.

5.2. Nusselt number and friction factor vs. slat angle and Reynolds number

The Nusselt number and friction factor would vary with the slat angle and Reynolds number. The *Nu* data obtained was shown in Fig. 8 and 9. It can be seen that increasing the slat angle resulted in decrease in Nusselt number for Reynolds number in the range of 4173–11,327. For Reynolds number above 13,116, the Nusselt number increases slightly firstly with the slat angle increasing from 5° to 10°, and afterwards it experiences a decreasing trend with the increased of the slat angle. For any certain slat angle, the Nusselt number increases with the increase in Reynolds number. This phenomenon is mainly due to higher Reynolds number helped increase turbulence in the flow. The correlation between the Nusselt number and the characteristic parameters can be expressed as

$$Nu = \begin{cases} 1.9549Re^{0.448}\left(\theta/90^{\circ}\right)^{-0.004}, 5^{\circ} \le \theta \le 15^{\circ} \\ 1.5199Re^{0.461}\left(\theta/90^{\circ}\right)^{-0.084}, 15^{\circ} < \theta \le 55^{\circ} \\ 1.9609Re^{0.422}\left(\theta/90^{\circ}\right)^{-0.259}, 55^{\circ} < \theta \le 85^{\circ} \end{cases} \quad (6)$$

for *Re* in the range of 4373–13,116.

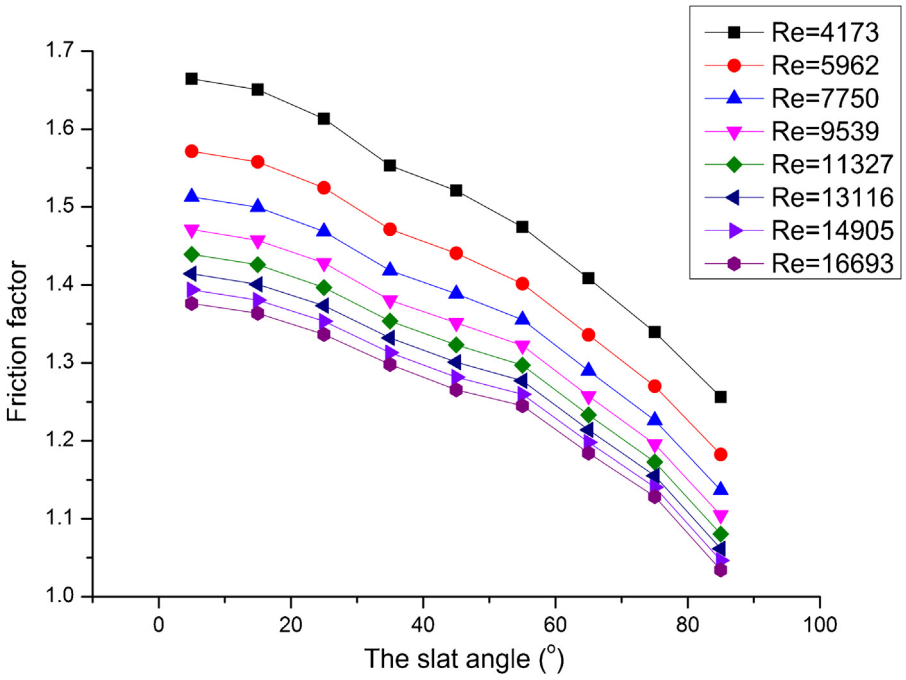

Fig. 10. Dependence of Friction factor on the slat angle.

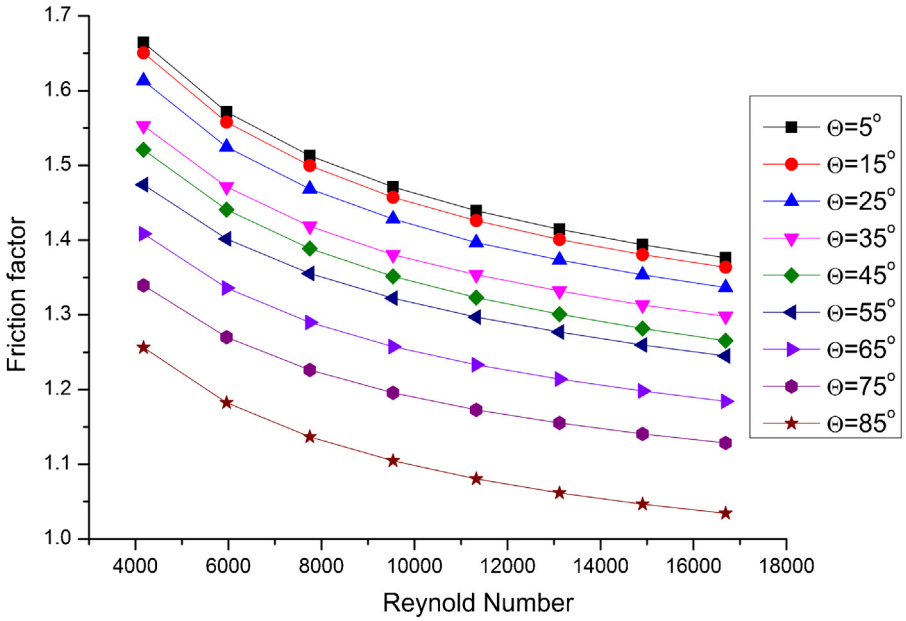

Fig. 11. Dependence of Nusselt number on Reynold number.

It can be seen that the Nusselt number is proportional to the range of 0.422–0.461 power of the Reynolds number. The effect of the slat angle on the Nusselt number is larger at high slat angle than that at small slat angle. The maximum deviation between the Nusselt number obtained from the CFD simulation and the number predicted using Eq. (2) is 3.89%, while the mean deviation is 1.39%.

The friction factor data obtained was shown in Fig. 10 and 11. Due to laminar sub-layer suppression, either increasing the Reynolds number or slat angle would make the friction factor decrease. The relation between the friction factor and the characteristic parameters can be expressed by using the following equation

$$f = \begin{cases} 5.0432Re^{-0.1366}\left(\theta/90^{\circ}\right)^{-0.008}, 5^{\circ} \le \theta \le 15^{\circ} \\ 4.2465Re^{-0.1317}\left(\theta/90^{\circ}\right)^{-0.094}, 15^{\circ} < \theta < 55^{\circ} \\ 3.3706Re^{-0.1224}\left(\theta/90^{\circ}\right)^{-0.409}, 55^{\circ} \le \theta \le 85^{\circ} \end{cases} \quad (7)$$

for Re in the range of 4373–13,116.

Using Eq. (3), the friction factor values at the simulated Reynolds number for all the slat angles were evaluated. The maximum deviation between the predicted valued and the CFD results is 2.3%, while the mean deviation is 0.74%.

6. Conclusion

In this study, a 2-dimensional CFD analysis has been carried out to determine the flow and heat transfer of the novel Trombe wall with venetian blind structure. The results of the present model were in good agreement with the experimental results. The effect of the different slat angles on the solar thermal efficiency, Nusselt number and friction factor are intensively investigated. The Reynolds number was arranged in the range of 4173–16,693. The results of this work are summarized as following:

(i) With the same solar radiation received by venetian blinds, smaller slat angle can help enhance the outlet air temperature and solar thermal efficiency, while increasing the Reynolds number leads to decrease in outlet air temperature and increase in solar thermal efficiency.
(ii) The Nusselt number value of the venetian blind increases with the increase of the Reynolds number value and decrease of the slat angle. The friction factor value decreases with the increase of the Reynolds number value and the slat angle.
(iii) The empirical equations of heat transfer and flow resistance are proposed. The Nusselt number is proportional to the range of 0.422–0.461 power of the Reynolds number. The effect of the slat angle on the Nusselt number is larger at high slat angle than that at small slat angle.

Acknowledgements

This research was supported by the grants from the Twelfth Five-year Science and Technology Support Key Project of China (No. 2012BAJ08B04), and DongGuan Innovative Research Team Program (No. 2014607101008).

References

[1] F. Abbassi, N. Dimassi, L. Dehmani, Energetic study of a Trombe wall system under different Tunisian building configurations, Energy Build. 80 (2014) 302–308.
[2] K.K.W. Wan, D.H.W. Li, D. Liu, J.C. Lam, Future trends of building heating and cooling loads and energy consumption in different climates, Build. Environ. 46 (1) (2011) 223–234.
[3] X.Q. Zhai, R.Z. Wang, Experiences on solar heating and cooling in China, Renew. Sustain. Energy Rev. 12 (4) (2008) 1110–1128.
[4] B. Li, R. Yao, Q. Wang, Y. Pan, An introduction to the Chinese Evaluation Standard for the indoor thermal environment, Energy Build. 82 (2014) 27–36.
[5] Z. Wang, R. de Dear, B. Lin, Y. Zhu, Q. Ouyang, Rational selection of heating temperature set points for China's hot summer—cold winter climatic region, Build. Environ. 93 (2) (2015) 63–70.
[6] X. Chen, H. Yang, L. Lu, A comprehensive review on passive design approaches in green building rating tools, Renew. Sustain. Energy Rev. 50 (2015) 1425–1436.
[7] A. Briga-Sá, A. Martins, J. Boaventura-Cunha, J.C. Lanzinha, A. Paiva, Energy performance of Trombe walls: adaptation of ISO 13790:2008(E) to the Portuguese reality, Energy Build. 74 (2014) 111–119.
[8] J. Shen, S. Lassue, L. Zalewski, D. Huang, Numerical study on thermal behavior of classical or composite Trombe solar walls, Energy Build. 39 (8) (2007) 962–974.
[9] M. Rabani, V. Kalantar, A.K. Faghih, M. Rabani, R. Rabani, Numerical simulation of a Trombe wall to predict the energy storage rate and time duration of room heating during the non-sunny periods, Heat Mass Transf. 49 (10) (2013) 1395–1404.
[10] L.F. Cabeza, C. Castellon, M. Nogues, M. Medrano, R. Leppers, O. Zubillaga, Use of microencapsulated PCM in concrete walls for energy savings, Energy Build. 39 (2) (2007) 113–119.
[11] L. Zalewski, A. Joulin, S. Lassue, Y. Dutil, D. Rousse, Experimental study of small-scale solar wall integrating phase change material, Sol. Energy 86 (1) (2012) 208–219.
[12] A.J.N. Khalifa, E.F. Abbas, A comparative performance study of some thermal storage materials used for solar space heating, Energy Build. 41 (4) (2009) 407–415.
[13] J. Jie, Y. Hua, P. Gang, J. Bin, H. Wei, Study of PV-Trombe wall assisted with DC fan, Build. Environ. 42 (10) (2007) 3529–3539.
[14] J. Jie, Y. Hua, H. Wei, P. Gang, J.P. Lu, J. Bin, Modeling of a novel Trombe wall with PV cells, Build. Environ. 42 (3) (2007) 1544–1552.
[15] T.T. Chow, J.W. Hand, P.A. Strachan, Building-integrated photovoltaic and thermal applications in a subtropical hotel building, Appl. Therm. Eng. 23 (16) (2003) 2035–2049.
[16] T.T. Chow, K.F. Fong, W. He, Z. Lin, A.L.S. Chan, Performance evaluation of a PV ventilated window applying to office building of Hong Kong, Energy Build. 39 (6) (2007) 643–650.
[17] W. Sun, J. Ji, C.L. Luo, W. He, Performance of PV-Trombe wall in winter correlated with south facade design, Appl. Energy 88 (1) (2011) 224–231.
[18] J. Han, L. Lu, J. Peng, H. Yang, Performance of ventilated double-sided PV façade compared with conventional clear glass façade, Energy Build. 56 (2013) 204–209.
[19] X. Hong, W. He, Z. Hu, C. Wang, J. Ji, Three-dimensional simulation on the thermal performance of a novel Trombe wall with venetian blind structure, Energy Build. 89 (0) (2015) 32–38.
[20] W. He, Z. Hu, B. Luo, X. Hong, W. Sun, J. Ji, The thermal behavior of Trombe wall system with venetian blind: an experimental and numerical study, Energy Build. 104 (2015) 395–404.
[21] FLUENT 6.3 User's Guide, Fluent Inc., 2006.
[22] J.A. Duffie, W.A. Beckman, Solar Engineering of Thermal Processes, Wiley, 1991.